ADVANCED FUNCTIONAL MATERIALS
www.afm-journal.de

Quantum Theory of Contact Electrification for Fluids and Solids

Morten Willatzen, Lok C. Lew Yan Voon, and Zhong Lin Wang*

A unified quantum-mechanical model of contact electrification that provides a microscopic basis for the Volta–Helmholtz–Montgomery hypothesis is presented. The model can represent metals, semiconductors, or insulators, in either fluid or solid phase, and with an effective electron transfer parameter as the driving mechanism. Known experimental results such as the charging of similar materials, the charging of similar materials with different contact orientation, the surface charge mosaic, and the higher efficiency of charge transfer for a liquid–solid contact, compared to a solid–solid one, are reproduced. A quantum-mechanical charge oscillation in the femtosecond to picosecond regime is predicted to take place. Coulomb interaction is found to have an impact on not just the charge transferred but also the period of charge oscillation.

1. Introduction

Triboelectricity, the generation of electrostatic charge via contact or friction, is a natural phenomenon tamed by man since the early days and put to good use in technologies such as laser printing[1,2] though still disruptive in natural and industrial environments, proposed as a clean form of energy via triboelectric nanogenerators,[3–6] and even to date contains fundamental surprises such as the observed generation of X-rays by peeling adhesive tape.[7] Yet, triboelectricity has escaped much quantitative analysis and it has been rather challenging to propose a unified physical model that covers such a broad range of materials.[8] This is primarily due to two factors: 1) It involves multiple and multiphysics processes (e.g., mechanical deformation, electric charge transport, carrier heating, ...), and 2) it is not an intrinsic material property but depends on many external conditions such as surface roughness, environmental conditions, ... It is, therefore, clear that any meaningful theory and quantitative analysis need to remove as many of the variables as possible. An example of this approach is the recent standardization of the triboelectric series (i.e., a predictive scale) by using a reference standard since two materials are needed to generate the effect and by using the liquid phase for the reference material since this allows the almost complete removal of the surface morphology variable.[9]

Our focus in this paper is on the subset of triboelectric phenomena known as contact electrification (CE), i.e., electrification without the need for friction. The experimental investigation of CE has been well documented by Harper.[10] It has advanced somewhat in recent years, since the introduction of Kelvin probe force microscopy.[11] On the theory side, one still relies predominantly on the qualitative picture of CE provided by the Volta–Helmholtz hypothesis for understanding electron transfer[10,12,13] that contact is required for electrification, and that a double charge layer is formed as a result, leading to a contact potential difference. This has been refined by the scheme in terms of band energies introduced by Vick[14] and Montgomery[15] and we refer to this state of knowledge as the Volta–Helmholtz–Montgomery hypothesis, and this is described pictorially in **Figure 1**. They sought to establish the why of CE and led to the widely accepted band picture for different types of solid contacts.

For example, for metal–metal contacts, charge transfer is postulated to occur due to Fermi-level differences whereas, for metal–insulator contacts, empty surface states on the insulator side are needed. A modern scheme in terms of the electron-cloud overlap has been proposed but is illustrative only.[8]

We have found three distinct types of modeling of CE to date: classical, phenomenological, or density-functional calculations. The work of Duke and Fabish[16,17] sought to establish the validity of the Montgomery scheme by using 1) ab initio calculations to identify the existence of discrete levels on the

Prof. M. Willatzen, Prof. Z. L. Wang
CAS Center for Excellence in Nanoscience
Beijing Key Laboratory of Micro-Nano Energy and Sensor
Beijing Institute of Nanoenergy and Nanosystems
Chinese Academy of Sciences
Beijing 100083, P. R. China
E-mail: morwi@fotonik.dtu.dk

Prof. M. Willatzen, Prof. Z. L. Wang
School of Nanoscience and Technology
University of Chinese Academy of Sciences
Beijing 100049, P. R. China

Prof. M. Willatzen
Department of Photonics Engineering
Technical University of Denmark
DK-2800 Kongens Lyngby, Denmark

Prof. L. C. Lew Yan Voon
Department of Physics
University of West Georgia
Carrollton GA 30118, USA

Prof. Z. L. Wang
School of Materials Science and Engineering
Georgia Institute of Technology
Atlanta GA 30332-0245, USA

The ORCID identification number(s) for the author(s) of this article can be found under https://doi.org/10.1002/adfm.201910461.

DOI: 10.1002/adfm.201910461

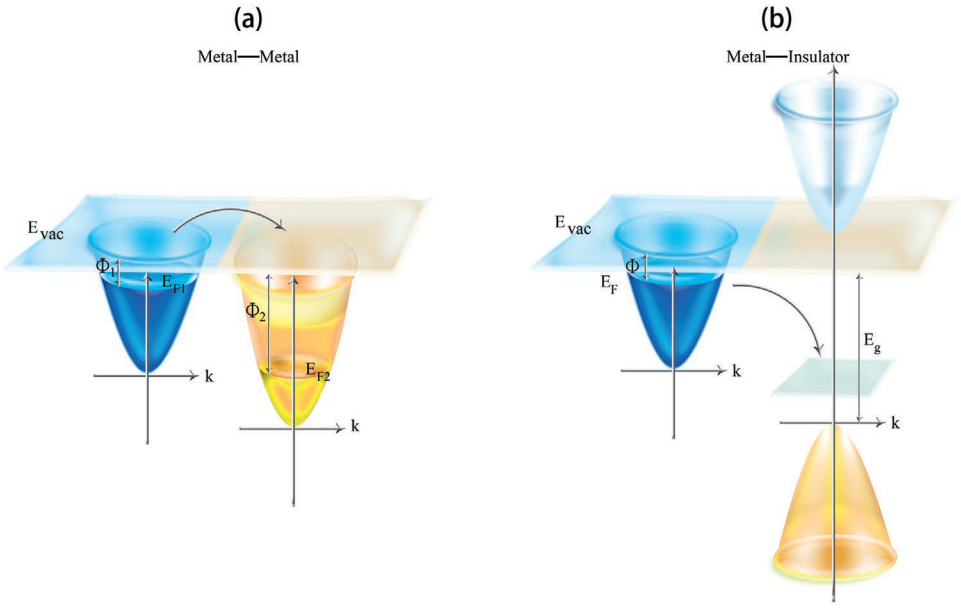

Figure 1. Volta–Helmholtz–Montgomery hypothesis shown for a) metal–metal and b) metal–insulator.

insulator side of a metal–insulator junction (as intrinsic localized molecular-ion levels to explain charge transfer for metal–polymer[16]) and 2) a fitted energy structure and density-of-states to calculate charge transfer in polymer–polymer contacts.[17] Two of the more recent models sought to provide a driving mechanism for CE. Lacks et al.[18] sought to explain charging of the same materials via a rate equation model where the driving mechanism was artificially introduced by putting constraints on which transfers are allowed without any microscopic basis and the model parameters were randomly chosen. More recently, flexoelectricity was introduced to explain charging due to indentations[19] yet the model ignored potentially more significant effects such as piezoelectricity, had electric potential estimates that were rather large, and is clearly not applicable for situations when flexoelectricity is not operative (e.g., for CE in general). We note that all of the above models lacked predictions. As to be expected, first-principles calculations [and mostly density-functional theory (DFT)] have been carried out for quantitative studies but do not provide explanations for all observed effects and are currently restricted to periodic solids and elastic electron transfer.[20–26] Indeed, it is even questionable as to whether they all computed charge transfer. For example, Zhang and Shao[22] clearly did not since they relaxed a system consisting of both materials—this amounts to bond creation between the two materials and the "charge transfer" they calculated is simply a bond polarity. On the other hand, Wu et al.[25] did a very careful analysis and uncovered a possible regime where the driving force is electrostatic. In general, while DFT is a great semipredictive tool, it is much very like an experimental tool, requiring other models and theories to analyze its results. Therefore, a more general and quantitative microscopic model that can simulate a wide variety of materials and phenomena for CE is still missing.

In this paper, we propose the first such unifying physical model. We focus on the electron transfer (as opposed to ion and material transfer), contact electrification (instead of frictional), and do not consider environmental factors such as humidity. Beyond that, the model is very general in being applicable to a variety of materials and transfer mechanisms. As many CE researchers have observed,[18,19] a "driver" for electron transfer is needed. The most fundamental one for electrons is the Hamiltonian quantum dynamics. Our group has started a quantum-mechanical study of CE by computing two possible mechanisms of electron transfer: 1) quantum tunneling across a gap[27] and 2) the photon-assisted transition rate.[28] The lossless quantum tunneling mechanism between essentially two bulk metals did allow for the explicit calculation of the charge transfer. In the current work, we are generalizing the above work to treat more general contacts by introducing a new quantum-mechanical model based on localized orbitals instead of Bloch states. This allows us to study practically any kind of contact and display a time dynamics not previously studied.

2. Basic Model

2.1. Scheme

Montgomery's theoretical scheme is based on seven assumptions.[15] Our scheme of contact electrification consists of the following elements:

- Only electron transfer occurs.
  Our goal is to demonstrate quantitatively the phenomenon of electron transfer when two materials are brought together and separated. Thus, we are automatically excluding systems whereby ions might be involved (e.g., in the presence of an ionic fluid); it is now indeed believed that most CE involves electron transfer.[8,29,30]
- A microscopic quantum-mechanical model is introduced.
  The most fundamental approach to studying electron dynamics is by defining an appropriate Hamiltonian and solving the

time-dependent Schrödinger equation. Our Hamiltonian models a system consisting of two materials with a coupling between them in order to represent the electronic charge transfer. The coupling will be described by an effective hopping parameter t_C, which can be chosen to describe various electron transfer mechanisms such as quantum tunneling, photon-assisted, phonon-assisted, ... Additionally, it could account for the imperfect contact between solids as well as the separation of contacts after charging.

- It can be chosen to model both solid–solid and fluid–solid contacts, as well as differentiating between metal–metal, metal–insulator, metal–semiconductor, and insulator–insulator contacts.
- A 1D version is implemented.
  This apparent restriction is to simplify the model computationally as much as possible while retaining much of the physics. Indeed, it is known that "any quantum-mechanical model can be transformed into one or more chain models."[31] Hence, even the differing surface physics associated with crystal faces of different orientations can be modeled by using chains with differing hopping parameters. 1D models are often used in physics, such as in a model of frictional electrification via electron–phonon interaction.[32] It could also be relevant to modeling 1D arrays of electrostatically charged spheres.[33]

While the model lacks a few features such as multiple energy bands, it does contain the most fundamental physics and should, therefore, display the key properties of CE without the need to introduce thermal or flexoelectric driving forces to account for CE. As P. W. Anderson said in his 1977 Nobel lecture, "Very often such, a simplified model throws more light on the real workings of nature than any number of 'ab initio' calculations."

2.2. Hamiltonian

The 1D model is depicted in **Figure 2**. The system of two materials in proximity to each other is described by a Hamiltonian $H = H_L + H_R + H_C$, which consists of three tight-binding (TB)-like components.[34] Each of the component Hamiltonians is given by a nearest-neighbor TB approximation to describe the coupling of two finite systems composed of either two solids or a solid and a fluid. The starting point is then the TB Hamiltonian

$$H = \sum_{l=0}^{N} \left[t_l \left(a_l^\dagger a_{l+1} + a_{l+1}^\dagger a_l \right) - e\phi_l a_l^\dagger a_l \right] \tag{1}$$

where l labels the atomic sites and

$$\begin{aligned} &t_l = 0, \text{ if } l = 0 \\ &t_l = t_L, \text{ if } 1 \le l \le M-1 \\ &t_l = t_C, \text{ if } l = M \\ &t_l = t_R, \text{ if } M+1 \le l \le N-1 \\ &t_l = 0, \text{ if } l = N \end{aligned} \tag{2}$$

are the hopping amplitudes, ϕ_l is the scalar electric potential at site l (refer to the next section), and e is the positive elementary charge. At the boundary sites $l = 1$ ($l = N$), the hopping amplitudes to the left (right) are zero. A barrier layer separating the two materials is placed between sites M and $M + 1$. Hopping across the barrier layer is described by the hopping amplitude t_C. The sites $1 \le l \le M$ correspond to the left material L and $M + 1 \le l \le N$ to the right material R. We allow for different hopping amplitudes t_L and t_R in the left and right materials. More generally, the t_i within each material do not have to be the same in order to account for the reduction in periodicity for fluids and polymers. This representation of the Hamiltonian is obtained if one uses Wannier orbitals. While a TB basis is most efficient for narrow-band materials, in its parameterized formulation,[35] it can be used to reproduce the electronic structure of metal, semiconductors, and insulators alike. Such a Hamiltonian has been used in many branches of physics,[36] including more recently in the discovery of topological insulators in 2D materials.[37]

The coupling parameter t_C is a critical one in our model since it can be chosen to model different physical processes. For quantum tunneling, since the hopping parameter in a TB model leads to spatial electron transfer, it can be introduced to parameterize tunneling with no energy change of the electron. Photon-assisted and phonon-assisted tunneling can be handled by treating t_C as an effective parameter. Indeed, this is the missing "driver" for CE as sought by others.[18,19] Given that we have not explicitly included repulsive forces and our model is based on lattice sites, we have not attempted to explore the regime where others have found tunneling to be less significant than electrostatic forces.[25] It also quantifies the driving mechanism associated with electron-cloud overlap.[8,30] One could introduce surface corrugations by rescaling t_C

$$t_C' = \alpha t_C \tag{3}$$

The parameter α would then be related to the ratio of the contact cross-sectional area of the solid–solid interface to the fluid–solid interface (**Figure 3**).

For cleaved solid surfaces, the ratio can be taken to be 1 but, otherwise, a typical solid surface is very rough with features up to micrometer in depth.[10] For such large gaps, there is practically no quantum tunneling of either electrons or ions; hence, the charge transfer should be significantly reduced for a typical solid–solid contact versus a fluid–solid contact. In addition to modeling the initial contact charging, we can also model the charge transfer as the two materials are separated if the coupling mechanism is distance dependent. For example, there will be a reduced quantum tunneling as the separation increases.

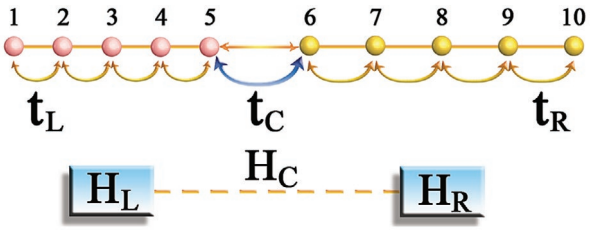

Figure 2. Top: 1D model of two materials in contact (shown with a total of 10 atoms as an example). Here, atoms 1–5 form the left (L) material and atoms 6–10 form the right (R) material. Bottom: a schematic of the Hamiltonian of the system, consisting of the tight-binding Hamiltonian of the left and right materials, coupled via a hopping parameter t_C.

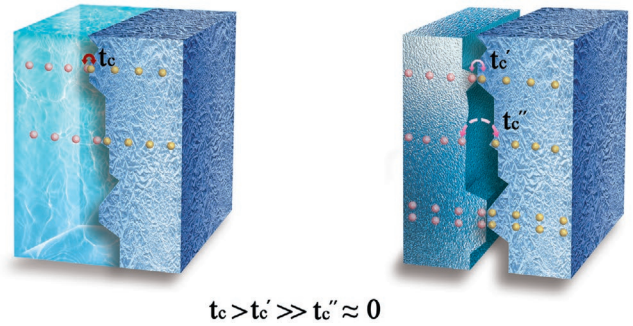

Figure 3. Contact microstructure for typical a) fluid–solid and b) solid–solid contacts.

Mathematically, this can be represented by a decreasing hopping parameter t_C. One can use the Harrison rule[38] to simulate the latter

$$t_C(t) = t_C\left(\frac{\mathrm{d}}{\mathrm{d}(t)}\right)^2, \quad \text{with} \quad \mathrm{d}(t) = d + vt \tag{4}$$

with the two materials separating with relative speed v. Finally, a note about the form of the electron interaction in Equation (1). We have used the simplified effective Coulomb interaction rather than the full many-body form.[39] The latter is a complex, unsolvable problem without approximations and we believe including the additional effect of electron correlation would detract from the main messages of this work without changing the basic physics being elucidated. We similarly used a 1D model in order to present the basic physics in an analytical or semianalytical form. Adding electron correlation to a 1D model could lead to a Coulomb blockade effect that would not occur in real 3D contacts and, hence, lead to an unphysical result. It can be expected that the main impact of electron correlation would be a change in the magnitude of charge transferred; for a model calculation that is not being compared to experimental data, this is not critical. Electron correlation effects can be subsequently included into the TB formalism.[40]

2.3. Solution

Let us write a general electronic quantum state as

$$|\psi(t)\rangle = \sum_{l=1}^{N} c_l(t)\,|l\rangle \tag{5}$$

where $c_l(t)$ are time-dependent coefficients determined by the Schrödinger equation

$$H\,|\psi(t)\rangle = i\hbar\,|\psi(t)\rangle \tag{6}$$

Multiplying Equation (6) on the left by $|n\rangle$ yields

$$i\hbar\dot{c}_n = t_n c_{n+1} + t_{n-1}c_{n-1} - e\phi_n c_n\,,\ 1 \le n \le N \tag{7}$$

which can be written out as

$$\begin{aligned}
&i\hbar\dot{c}_1 = t_1 c_2 - e\phi_1 c_1\\
&i\hbar\dot{c}_2 = t_1 c_3 + t_1 c_1 - e\phi_2 c_2\\
&\cdot\cdot\\
&i\hbar\dot{c}_M = t_C c_{M+1} + t_{M-1}c_{M-1} - e\phi_M c_M\\
&i\hbar\dot{c}_{M+1} = t_{M+1}c_{M+2} + t_C c_M - e\phi_{M+1}c_{M+1}\\
&\cdot\cdot\\
&i\hbar\dot{c}_{N-1} = t_{N-1}c_N + t_{N-2}c_{N-2} - e\phi_{N-1}c_{N-1}\\
&i\hbar\dot{c}_N = t_N c_{N+1} + t_{N-1}c_{N-1} = t_{N-1}c_{N-1} - e\phi_N c_N
\end{aligned} \tag{8}$$

where $t_N = 0$ was used in obtaining the second equality in the last expression. It now follows from Equation (2) that this system can be rewritten as

$$\begin{aligned}
&i\hbar\dot{c}_1 = t_L c_2 - e\phi_1 c_1\\
&i\hbar\dot{c}_2 = t_L c_3 + t_L c_1 - e\phi_2 c_2\\
&\cdot\cdot\\
&i\hbar\dot{c}_M = t_C c_{M+1} + t_L c_{M-1} - e\phi_M c_M\\
&i\hbar\dot{c}_{M+1} = t_R c_{M+2} + t_C c_M - e\phi_{M+1}c_{M+1}\\
&\cdot\cdot\\
&i\hbar\dot{c}_{N-1} = t_R c_N + t_R c_{N-2} - e\phi_{N-1}c_{N-1}\\
&i\hbar\dot{c}_N = t_R c_{N-1} - e\phi_N c_N
\end{aligned} \tag{9}$$

This system of linear first-order equations in time can be easily solved numerically subject to specified initial conditions

$$c_l(0) = c_l^0\,,\ 1 \le l \le N \tag{10}$$

Electrostatic effects due to charge build up are clearly important. This has earlier been shown to limit the maximum charge transfer.[41,42] Coulomb interactions due to hopping electrons are accounted for as follows. The scalar electric potential at site l, ϕ_l, is the sum of contributions from charged infinite planes located at the sites m

$$\begin{aligned}
&\phi_l = \phi(z_{\mathrm{ref}}) - \sum_{m=1}^{N}\frac{\sigma_m}{2}\int_{z_{\mathrm{ref}}}^{z_l}\frac{1}{\epsilon(z')}\,\mathrm{sign}(z'-z_m)\,\mathrm{d}z'\\
&\sigma_m = -\frac{e}{A}\left(|\,c_m(t)\,|^2 - |\,c_m(0)\,|^2\right)
\end{aligned} \tag{11}$$

where A is the area per 1D chain and $|c_m(t)|^2$ denotes the m'th site electron occupancy at time t. The difference $(|c_m(t)|^2 - |c_m(0)|^2)$ reflects that initially ($t = 0$) all sites are assumed electrically neutral. Hence, at $t = 0$, the electron charge at site l is exactly compensated by a positive (and fixed in time) ionic charge at the same site. As the electrons move about, the difference $(|c_m(t)|^2 - |c_m(0)|^2)$ is generally nonzero and a scalar electric potential builds up. The scalar potential is set to ϕ_{ref} at position z_{ref}. Note that the influence of magnetic fields is discarded here and in the following.

In Equation (11), the permittivity ϵ is assumed step-wise constant, i.e., a constant in the left, right, and barrier materials

$$\begin{aligned}
&\epsilon(z) = \epsilon_L,\ \text{if } 1 \le l \le M-1\\
&\epsilon(z) = \epsilon_C,\ \text{if } l = M\\
&\epsilon(z) = \epsilon_R,\ \text{if } M+1 \le l \le N
\end{aligned} \tag{12}$$

and the sign function fulfills

$$\begin{aligned}
&\mathrm{sign}(z) = -1 \text{ if } z < 0\\
&\mathrm{sign}(z) = 1 \text{ if } z > 0
\end{aligned} \tag{13}$$

For metals, we have found it appropriate to set the permittivity to a very large value to represent the realistic situation of no interior electric field. This results in surface charges only and a simple expression for the Coulomb potential. Thus, for

$$\begin{aligned} &z_l \le z_M : \phi(z_l) = \phi(z_{\text{ref}}) \\ &z_M \le z_l \le z_{M+1} : \phi(z_l) = \phi(z_{\text{ref}}) - \sum_{m=1}^{M} \frac{\sigma_m}{\epsilon_C}(z_l - z_M) \\ &z_l \ge z_{M+1} : \phi(z_l) = \phi(z_{\text{ref}}) - \sum_{m=1}^{M} \frac{\sigma_m}{\epsilon_C}(z_{M+1} - z_M) \end{aligned} \tag{14}$$

In the above, we have used the charge neutrality condition

$$\sum_{m=1}^{M} \sigma_m = -\sum_{m=M+1}^{N} \sigma_m \tag{15}$$

This result leads to much more effective computation.

2.4. No Coulomb approximation

It is worthwhile analyzing first the solutions in the absence of Coulomb interaction. The system of equations can be solved either as an eigenvalue problem or by discretizing in time. In the former case, the set of equations can be written in matrix form, with the latter being tridiagonal. If all the hopping and onsite parameters are the same (so-called uniform case), the matrix is of the Toeplitz type[36,43,44] and have been extensively studied in the mathematical literature.

The eigenvalues are known to come in pairs $\pm\lambda_i$ if the matrix is even-dimensional and with an additional zero eigenvalue if odd-dimensional for the uniform case. In our case, such behavior governs the time dynamics since any arbitrary solution can be written as a linear combination of these eigensolutions at finite time, with the initial condition determining the expansion coefficients. Thus, the time dynamics of our system, even in the absence of Coulomb interaction, should not in general display a simple periodic motion. Such a complex time dynamics will be evident in our numerical solutions.

2.5. General solution

The coupled first-order differential equations are solved using the finite-difference approximation. Typical time steps used were 3×10^{-5} in units of $h\,\text{eV}^{-1} = 4.17\,\text{fs}$. It was found through testing that a larger time step leads to numerical instability. One of the approaches to checking for the numerical stability of the computation is by calculating the total charge as a function of time. Most of the results to be presented were carried out using a total of 10–30 atomic sites.

3. Calculations

3.1. Parameters

Our 1D model of two materials in contact can now be used to simulate a variety of commonly encountered triboelectric systems. This is carried out by using different hopping parameters t_i, dielectric constants ϵ_i, and starting electron distribution $c_i(0)$. For the transfer mechanism, we will only explicitly consider the case of quantum tunneling here; other mechanisms can be simulated by the appropriate choice of the hopping parameters. In line with the work of Duke and Fabish,[16,17] we assume insulators to consist of discrete levels and disorder leads to an energy spread of the levels (ensuring the possibility of lossless tunneling) and a site localization (hence the applicability of our model in terms of Wannier functions). Nonetheless, we have simplified our numerical calculations by only keeping one atomic site for the insulator and a priori assume the level alignment. The different general choices of parameters for the metal–metal, metal–insulator, and insulator–insulator problems are given in **Table 1**.

We start explaining the case of a fluid in contact with a solid since we can assume that the true contact area is the macroscopic cross-sectional area. The fluid is conventionally listed as the left (L) material. Liquid mercury (Hg) is often used as the fluid.[9,10] Hence, one can choose the value of the hopping parameter t for a metal to be that of Hg. This can be estimated by using the Harrison universal hopping parameters,[39] e.g.

$$t = V_{ss\sigma} = -1.32\,\frac{\hbar^2}{md^2} \tag{16}$$

where d is the bond length for the solid and can be chosen to be the first peak in the radial distribution function for a liquid. Both are known to be about the same (e.g., comparing for liquid sulfur at 500 K and solid sulfur at 300 K), which makes sense given the small volume change upon melting for most materials. For Hg, $d = 3$ Å. This gives $t \approx -1$ eV (t_L). We now explain the choice of the other parameters for each case.

- Metal–metal. t_R and t_L can be chosen to be different to represent different metals; t_C is generally chosen smaller to represent a weaker coupling at the interface. Since $\sum_i |c_i|^2$ can be chosen as a measure of the charge density and, therefore, the chemical potential, we pick it to be <1 in a metal to represent an unfilled band.
- Metal–insulator. Generally, the metal work function is higher than the electron affinity of an insulator, leading to no contact charging unless other states are involved such as surface states[14] or molecular-ion states.[16] Assuming such a mechanism and that the localized states are confined to the layer

Table 1. Parameters for contacts studied.

	Metal–metal	Metal–insulator	Insulator–insulator
t_L[eV]	−1.0	−1.0	0.0
t_C[eV]	-0.75α	-0.75α	$-\alpha$
t_R[eV]	−1.0	0.0	0.0
ϵ_L	∞	∞	1.0
ϵ_C	1.0	1.0	1.0
ϵ_R	∞	1.0	1.0
$c_L(0)$	c_L	c_L	0.0
$c_C(0)$	c_L	c_L	c_C
$c_R(0)$	c_R	0.0	0.0

right at the contact, this means all $t_R = 0$ if the electrons are trapped there. The starting wave function is chosen to represent an electron on the left.
- Insulator–insulator. This case is modeled with only hopping at the interface and with the electron starting to the left of the interface.

For the solid–solid contact, the true surface area can be much smaller than the apparent one. This is achieved by scaling down the hopping parameters by α.

3.2. Results

We report below example calculations carried out using specific values of the parameters in Table 1. In all cases, we calculated what Montgomery called q_0, "the charge transferred initially upon contact."[15] All of the material systems studied display the key phenomena of interest in this paper and so the latter will not be repeated for all systems.

3.2.1. Insulator–Insulator

We present first the insulator–insulator case since the problem reduces to having only two sites (**Figure 4**). This case also has an exact analytical solution when the Coulomb interaction is not included

$$c_C(t) = c_C(0)e^{-it_C t/\hbar},\ c_R(t) = c_R(0)e^{-i(t_C t/\hbar+\phi)} \tag{17}$$

where c_C and c_R are the wave functions on the two sites forming the contact. This solution shows that there is a natural charge oscillation with a frequency proportional to the hopping parameter; for $t_C = -1\,\text{eV}$, $f = h\,\text{eV}^{-1} = 0.24\,\text{fs}^{-1}$. It is analogous to the Rabi frequency, which is proportional to the dipole matrix element. Numerical calculations inclusive of the Coulomb interaction show that the oscillation is preserved (Figure 4). In the figures, we define charging to be a measure of charge transfer in units of electron charge

$$\text{charging} = -\sum_{m=1}^{N_L}(|c_m(t)|^2 - |c_m(0)|^2) \tag{18}$$

Note that the two insulators are taken to be different materials in order to generate charge transfer in this two-site model (one site per material because the hopping parameter is set to zero for an insulator). This is simulated by choosing different starting charge population on the two sites (0.01 and 0, respectively), even though both materials are electrically neutral to start with. We used a total of $N = 10$ sites, with $N_L = N_R = 5$ for each material, for numerical convenience though the results can be extended to larger N. In order to simulate the reduced contact area of the solid–solid contact with respect to the fluid–solid case, we used $\alpha = 0.1$; for rough surfaces, this ratio would be even smaller. The main features of our results (Figure 4) are as follows:

1) Charge oscillates back and forth due to the hopping coupling, and the transfer rate is enhanced by the presence of the Coulomb interaction. It remains in the femtosecond regime and should be observable in time-resolved experiments.
2) At low carrier concentration, Coulomb effects are unimportant and the exact results given in Equation (17) are valid. For example, the period of charge oscillation is proportional to αt_C and maximum charge transfer is 100% irrespective of αt_C. Hence, the use of α alone is not an appropriate representation of true contact area.
3) At high concentration, maximum charge transfer went down from 100% to about 3.5% and the period of oscillation decreased almost tenfold. When α is increased from 0.1 to 1, the maximum charge transfer increased to about 15% and the period is much lower. In this case, α could be used to represent the true contact area.

The above results demonstrate "isoenergetic" charge transfer between two similar insulators provided there is a coupling between the two systems. We believe this is an appropriate model of the polymer–polymer system studied by Duke and Fabish.[17] Our numerical results indicate that the use of α is, in general, insufficient to account for the difference in contact area between the solid–solid and fluid–solid contacts; the latter can, nevertheless, be incorporated into our model either by modifying the initial electron concentration or a posteriori by multiplying by the area factor. We predict the quantum-mechanical oscillation of the charge transfer between the two materials. This phenomenon has not yet been observed, possibly because of dissipative processes involved in the experiments and the time scales involved.

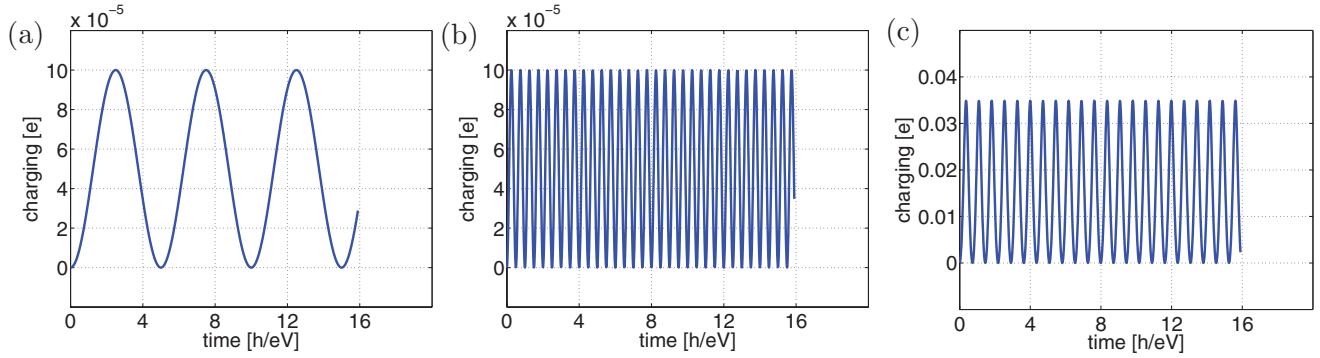

Figure 4. Insulator–insulator contact ($N_L = N_R = 5$): a) solid–solid ($\alpha = 0.1$, $c_C = 0.01$), b) fluid–solid ($\alpha = 1$, $c_C = 0.01$), and c) high carrier concentration, solid–solid ($\alpha = 0.1$, $c_C = 1.0$).

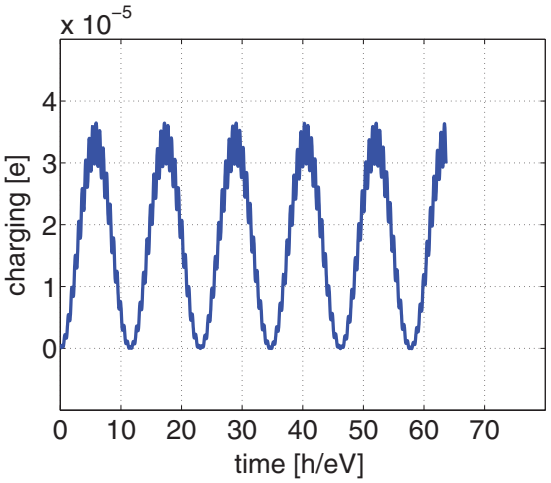

Figure 5. Metal–insulator contact ($N_L = N_R = 5$): solid–solid ($\alpha = 0.1$).

3.2.2. Metal–Insulator

The metal–insulator results are given in **Figure 5** for $N_L = N_R = 5$ and the solid–solid case, with $c_L = 0.01$ and $c_R = 0$. We simulate the difference in chemical potential before contact by setting different electron population on the two sides initially. When the hopping is turned on, we see a similar time dynamics as for the previous case of insulator–insulator but more complex due to the multiple time scales present as we earlier pointed out.

The charge transferred is not complete; in fact, with the chosen parameters, it is seen that about 8% of the original charge on the metal is transferred to the right (insulator), significantly lower than for the metal–metal case with the same overall dimension and t_C. This is consistent with what is seen experimentally.[12] In our model, this is seen to arise from the fact that the insulator has all the charge residing at the surface leading to strong Coulomb blockade, whereas they can spread out more for the metal.

3.2.3. Metal–Metal

An early puzzle for CE is the fact that charge transfer can also occur between similar materials. This was quickly attributed to the asymmetry being created by either different size and shape of the materials[8] or by other asymmetric effects such as rubbing[10] and temperature[12] although other mechanisms have been proposed.[18,19] Our model provides a very simple simulation of the size effect. We model the same (metallic) material on both sides (with $c_L(0) = c_R(0) = 0.01$) but with different thicknesses (**Figure 6**).

When the two materials have the same size ($N_L = N_R$), the charge transfer is zero. When the left material is made bigger, there is a net average charge transferred to the left, totaling about 92% of the total charge originally present on the right; the electrons are also seen to be transferred to the wider metal. Since the narrower layer has the opposite charge, the sign change due to different thicknesses. Thus, one can also propose this mechanism to explain the observed mosaic of charge signs on a single surface.[45] This is also a surface effect since a bulk property would not have a size dependence. If we artificially turn off the Coulomb interaction when the electron population is high enough, the charge transfer was found to be enhanced as there is no longer an opposing electric field to the charge build up. For example, with $c_L = c_R = 0.01 \times \sqrt{2}$, the transfer rate is reduced to 42%; if one turns off the Coulomb interaction, the maximum transfer rate reaches 100%. Hence, the total charge transferred depends not just on the geometry but also on the Coulomb interaction. The presence of multiple hopping parameters has again led to a complex time evolution.

On a final note, while all the examples presented in this paper involved system with a total of $N = 10$ sites, calculations with larger sizes yielded qualitatively similar results. An example of the metal–metal contact problem with $N_L = 10$, $N_R = 20$, i.e., a total of 30 sites is shown in **Figure 7**. The maximum charge transfer (to the right) is now about 35%.

4. Summary

We have developed a single, unifying, quantum-mechanical model that provides a framework for studying contact electrification due to electron transfer for different material systems. All these cases can be achieved by simply choosing different sets of three quantities: the hopping parameters between, and the dielectric constant and electron population on atomic sites.

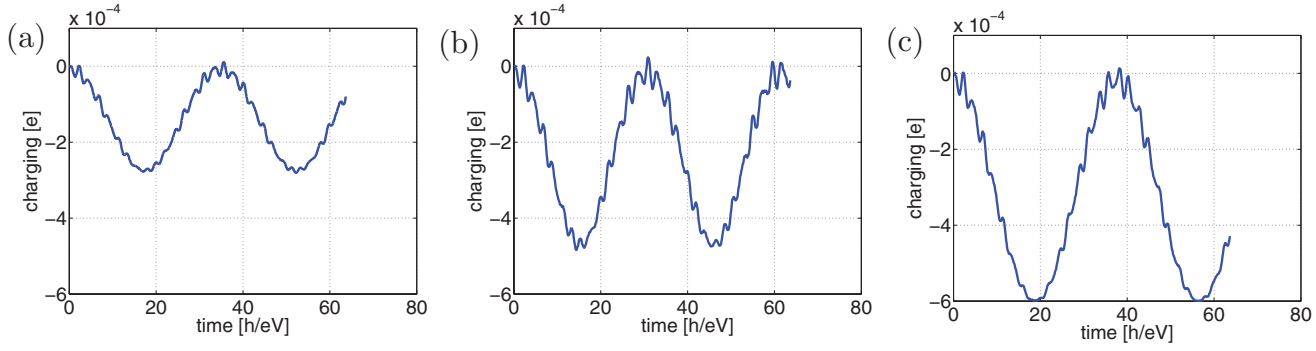

Figure 6. Metal–metal contact, solid–solid ($\alpha = 0.1$): $N_L = 7$; $N_R = 3$. a) With $c_L = c_R = 0.01$; b) with $c_L = c_R = 0.01 \times \sqrt{2}$; c) with $c_L = c_R = 0.01 \times \sqrt{2}$ and Coulomb turned off.

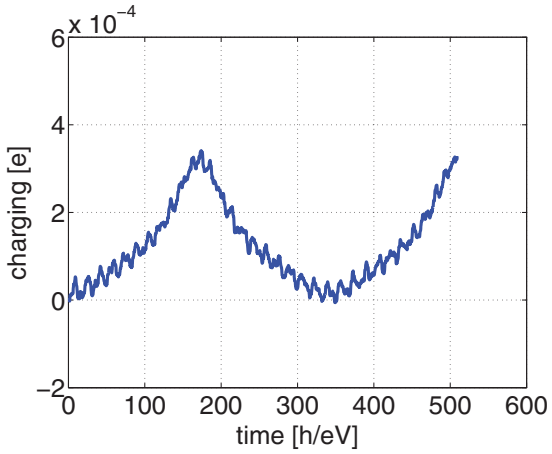

Figure 7. Metal–metal contact, solid–solid ($\alpha = 0.1$): $N_L = 10$; $N_R = 20$.

We have provided a microscopic and quantitative basis for the Volta–Helmholtz–Montgomery hypothesis, as well as quantified the electron-cloud-overlap picture for the driving mechanism. Our model predicts the possible existence of charge oscillations on the femtosecond to picosecond time scale (which could potentially be used to distinguish electron tunneling from other charge transfer mechanisms), provides explanations for the possibility of charge transfer for similar materials as well as the mosaic of charges for a given surface, quantifies the impact of Coulomb effects on limiting charge transfer, and demonstrates the significantly enhanced charge transfer for the fluid–solid contact compared to the solid–solid case.

Acknowledgements

The authors would like to thank Dr. Kong Xin for his help in organizing computer resources for carrying out this work. L.C.L.Y.V. would like to thank BINN for their hospitality. M.W. is grateful to the Talent 1000 Foreign Expert program for research funding.

Conflict of Interest

The authors declare no conflict of interest.

Keywords

contact electrification, Coulomb effects, quantum-mechanical models, quantum theory

Received: December 17, 2019
Revised: February 4, 2020
Published online: March 4, 2020

[1] P. E. Shaw, *Nature* **1926**, *118*, 659.
[2] L. B. Schein, *Science* **2007**, *316*, 1572.
[3] Z. L. Wang, L. Lin, J. Chen, S. Niu, Y. Zi, *Triboelectric Nanogenerators, Green Energy and Technology*, Springer, Berlin **2016**.
[4] J. Liu, A. Goswami, K. Jiang, F. Khan, S. Kim, R. McGee, Z. L. Li, Z. Hu, J. Lee, T. Thundat, *Nat. Nanotechnol.* **2018**, *13*, 112.
[5] R. Hinchet, H.-J. Yoon, H. Ryu, M.-K. Kim, E.-K. Choi, D.-S. Kim, S.-W. Kim, *Science* **2019**, *365*, 491.
[6] D. W. Kim, J. H. Lee, J. K. Kim, U. Jeong, *NPG Asia Mater.* **2020**, *12*, 6.
[7] C. G. Camara, J. V. Escobar, J. R. Hird, S. J. Putterman, *Nature* **2008**, *455*, 1089.
[8] Z. L. Wang,A. C. Wang, *Mater. Today* **2019**, *30*, 34.
[9] H. Zou, Y. Zhang, L. Guo, P. Wang, X. He, G. Dai, H. Zheng, C. Chen, A. C. Wang, C. Xu, Z. L. Wang, *Nat. Commun.* **2019**, *10*, 1427.
[10] W. R. Harper, *Contact and Frictional Electrification*, Clarendon Press, Oxford **1967**.
[11] W. Melitz, J. Shen, A. C. Kummel, S. Lee, *Surf. Sci. Rep.* **2011**, *66*, 1.
[12] J. Lowell, A. C. Rose-Innes, *Adv. Phys.* **1980**, *29*, 947.
[13] J. Henniker, *Nature* **1962**, *196*, 474.
[14] F. A. Vick, *Br. J. Appl. Phys.* **1953**, *4*, S1.
[15] D. J. Montgomery, in *Solid State Physics* (Eds: F. Seitz, D. Turnbull), Vol. 9, Academic Press Inc., New York **1959**, p. 139.
[16] C. B. Duke, T. J. Fabish, *Phys. Rev. Lett.* **1976**, *37*, 1075.
[17] C. B. Duke, T. J. Fabish, *J. Appl. Phys.* **1978**, *49*, 315.
[18] D. J. Lacks, N. Duff, S. K. Kumar, *Phys. Rev. Lett.* **2008**, *100*, 188305.
[19] C. A. Mizzi, A. W. Lin, L. D. Marks, *Phys. Rev. Lett.* **2019**, *123*, 116103.
[20] M. Yoshida, N. Ii, A. Shimosaka, Y. Shirakawa, J. Hidaka, *Chem. Eng. Sci.* **2006**, *61*, 2229.
[21] Y. Shirakawa, N. Ii, M. Yoshida, R. Takashima, A. Shimosaka, J. Hidaka, *Adv. Powder Technol.* **2010**, *21*, 500.
[22] Y. Zhang, T. Shao, *J. Phys. D* **2013**, *46*, 235304.
[23] X. Shen, A. E. Wang, R. M. Sankaran, D. J. Lacks, *J. Electrost.* **2016**, *82*, 11.
[24] S. Lin, T. Shao, *Phys. Chem. Chem. Phys.* **2017**, *19*, 29418.
[25] J. Wu, X. Wang, H. Li, F. Wang, W. Yang, Y. Hu, *Nano Energy* **2018**, *48*, 607.
[26] J. Wu, X. Wang, H. Li, F. Wang, Y. Hu, *Nano Energy* **2019**, *63*, 103864.
[27] M. Willatzen, Z. L. Wang, *Research* **2019**, *2019*, 6528689.
[28] M. Willatzen, Z. L. Wang, *Nano Energy* **2018**, *52*, 517.
[29] C.-Y. Liu, A. J. Baird, *Chem. Phys. Lett.* **2008**, *480*, 145.
[30] C. Xu, Y. Zi, A. C. Wang, H. Zou, Y. Dai, X. He, P. Wang, Y. C. Wang, P. Feng, D. Li, Z. L. Wang, *Adv. Mater.* **2018**, *30*, 1706790.
[31] R. Haydock, in *Solid State Physics* (Eds: H. Ehrenreich, F. Seitz, D. Turnbull), Vol. 35, Academic Press, New York **1980**, p. 215.
[32] S. Pan, Z. Zhang, *J. Appl. Phys.* **2017**, *122*, 144302.
[33] B. A. Grzybowski, A. Winkleman, J. A. Wiles, Y. Brumer, G. M. Whitesides, *Nat. Mater.* **2003**, *2*, 241.
[34] L. C. Lew Yan Voon, Ph.D. Thesis, Worcester Polytechnic Institute **1993**.
[35] J. C. Slater, G. F. Koster, *Phys. Rev.* **1954**, *94*, 1498.
[36] L. Banchi, R. Vaia, *J. Math. Phys.* **2013**, *54*, 043501.
[37] C. L. Kane, E. J. Mele, *Phys. Rev. Lett.* **2005**, *95*, 146802.
[38] W. A. Harrison, *Electronic Structure and the Properties of Solids*, Dover, Mineola, NY **1989**.
[39] H. Haug, S. W. Koch, *Quantum Theory of the Optical and Electronic Properties of Semiconductors*, World Scientific, NJ **2003**.
[40] E. Nielsen, R. Rahman, R. P. Muller, *J. Appl. Phys.* **2012**, *112*, 114304.
[41] D. J. Lacks, R. M. Sankaran, *J. Phys. D* **2011**, *44*, 453001.
[42] G. S. P. Castle, L. G. Schein, *J. Electrost.* **1995**, *36*, 165.
[43] D. Kulkarni, D. Schmidt, S.-K. Tsai, *Linear Algebra Its Appl.* **1999**, *297*, 63.
[44] W.-C. Yueh, *Appl. Math. E-notes* **2005**, *5*, 66.
[45] H. T. Baytekin, A. T. Patashinski, M. Branicki, B. Baytekin, S. Soh, B. A. Grzybowski, *Science* **2011**, *333*, 308.